

## Ytterbium Vanadate Nanomaterials: Solid State Fabrication, Characterization and Photocatalytic Degradation of MG Industrial Pollutant Under Visible Light Illumination

Leila Kafi-ahmadi <sup>1</sup> | Shahin Khademinia <sup>2</sup>

1. Correspond author, Department of Inorganic Chemistry, Faculty of Chemistry, Urmia University, Urmia, Iran. E-Mail: l.kafiahmadi@urmia.ac.ir
2. Department of Inorganic Chemistry, Faculty of Chemistry, Semnan University, Semnan, Iran E-Mail: khademinia Shahin@gmail.com

---

### Article Info

**Article type:**  
Research Article

**Article history:**

Received 8 September 2023  
Received in revised form 25  
November 2023  
Accepted 12 January 2024  
Published online 27 March  
2024

**Keywords:**

Nano-Photocatalyst,  
Ytterbium vanadate,  
Malachite Green,  
Rietveld.

---

### ABSTRACT

Ytterbium Vanadate nanopowders were utilized as a photocatalyst to eliminate contamination color under noticeable light illumination. The primary examination was tested by the FullProf program utilizing a profile coordinating with steady scale factors. The outcomes showed that the examples had a primary ytterbium vanadate structure with a space group of Fd-3m. FESEM pictures showed that the combined ytterbium vanadate particles had mono-molded circle morphologies. Photocatalytic execution of the incorporated nanomaterials was likewise examined for the debasement of poison MG under normal light illumination. The ideal circumstances were gotten by design expert programming. It was observed that the ideal condition was 0.07 mL H<sub>2</sub>O<sub>2</sub>, 0.02 g catalyst, 40 min. The yield in the condition was 77 %. The stock volume and concentration of MG were 70 mL and 50 ppm, respectively.

---

**Cite this article:** Kafi-ahmadi, L. & Khademinia, Sh. (2023). Ytterbium Vanadate Nanomaterials: Solid State Fabrication, Characterization and Photocatalytic Degradation of MG Industrial Pollutant Under Visible Light Illumination, *Advances in Energy and Materials Research*, 1 (1), 1-8. <https://doi.org/10.22091/jaem.2023.9833.1006>



© The Author(s).

DOI: <https://doi.org/10.22091/jaem.2023.9833.1006>

Publisher: University of Qom.

---

## 1. Introduction

In the current work, Photocatalytic utilization of the integrated ytterbium vanadate nanomaterials was additionally researched for the corruption of MG under regular light conditions. It was found that the integrated ytterbium vanadate nanocatalyst had great productivity under regular light. MG is characterized in the coloring business as an organic compound color and is utilized in shade application. The dye is utilized widely in several applications such as fisheries and the hydroponics industry [1, 2]. MG toxin color is not degraded biologically and has now turned into a profoundly dubious compound because of the dangers it postures to the purchasers of treated fish, remembering its belongings for the invulnerable and multiplication frameworks. Moreover, MG and its derivatives cause several diseases such as mutagenic, cancer-causing, and teratogenic impacts to living beings [3]. It ought not to be utilized for refreshments, food, or medications since it causes skin bothering, obscured vision, or cause impedance. Its inward breath might make disturbance the respiratory parcel, and in huge amounts make tissue harm and irritation to the kidneys [4]. pure and composite nanomaterials have been seen as a few reactant and photocatalytic applications [5,6]. As of late, a few metal oxides have been utilized for the corruption of MG under various circumstances that are included in ref [7-16]. To observe the ideal upsides of boundaries influence on MG photodegradation processes, a test plan technique is used. In the technique, a Design Of Expert (DOE) utilizing Central Composite Design (CCD) is applied. Plan of Expert is a piece of programming intended to assist with the plan and understanding of multifaceted analyses. In the present photocatalytic process, the product is applied to assist specialists with planning an investigation to perceive the amount of photocatalyst and  $H_2O_2$  utilized and how long time is expected to conclude the debasement interaction. The product suggests a wide scope of plans, such as factorials, partial factorials, and composite plans. Design Expert offers PC-created D-ideal plans for situations where standard plans are not pertinent, or where we wish to expand a current plan [17, 18]. A Box-Wilson Central Composite Design ordinarily called a focal composite plan, contains an embedded factorial or partial factorial plan with focus focuses that is increased with a gathering of focuses that permit assessment of ebb and flow. Assuming the separation from the focal point of the plan space to a factorial point is  $\pm 1$  unit for each variable, the separation from the focal point of the plan space to appoint is  $|\alpha| > 1$ . The exact worth of  $\alpha$  relies upon specific properties wanted for the plan and on the number of elements included [17, 18]. This work reports the intermolecular communications in the gem

design of  $Yb_2V_2O_7$  by Hirshfeld surface examination. Moreover, the photocatalytic execution of the combined  $Yb_2V_2O_7$  nanomaterial is explored for the debasement of MG under noticeable light conditions. Design expert technique is utilized to enhance factors influencing the corruption response. The elements are how much the nanocatalyst,  $H_2O_2$ , and the reaction time that affects the MG degradation yield.

## 2. Experimental

### 2.1. General Remarks

All synthetics were of insightful grade, acquired from business sources, and utilized minus any additional refinement. Crystal phase identification was done by a powder X-ray diffractometer D5000 (Siemens AG, Munich, Germany) that uses  $CuK\alpha$  radiation. The morphology of the fabricated samples was tested by a field emission scanning electron microscope instrument (Hitachi FE-SEM model S-4160). UV-Vis spectra were taken by an Analytik Jena Specord 40 (Analytik Jena AG Analytical Instrumentation, Jena, Germany). Estimation of the photocatalytic action of the combined  $Yb_2V_2O_7$  tests in the corruption of MG was explored within the sight of  $H_2O_2$  (35%, w/w) under visible light illumination.

### 2.2. Fabrication of $Yb_2V_2O_7$ Samples by Solid State Route

In a normal preparation experiment, 0.197 g (0.5 mmol) of  $Yb_2O_3$  ( $M_w = 394.00 \text{ gmol}^{-1}$ ) and 0.184 g (1.0 mmol) of  $Na_2VO_4$  ( $M_w = 183.91 \text{ gmol}^{-1}$ ) were blended in a mortar and ground until an almost homogeneous powder was acquired. The acquired powder was treated thermally in a 25 mL crucible in one stage at 300 ( $S_1$ ), 400 ( $S_2$ ), 500 ( $S_3$ ) and 600 °C for 8 h ( $S_4$ ). The sample was then cooled ordinarily in the furnace to the normal temperature. The acquired powder was gathered for additional examinations. A yellowish powder was acquired. The reaction yields were 92, 85, 88, and 91 % for  $S_1$ ,  $S_2$ ,  $S_3$ , and  $S_4$ , respectively.

## 3. Results and Discussions

### 3.1. Materials Characterization

The phase compositions of  $Yb_2V_2O_7$  nanomaterials were analyzed by powder X-ray diffraction method. Figure 1(a-d) shows the PXRD examples of the acquired materials in the  $2\theta$  territory 10-90° as well as the FullProf program was used for primary examinations on crystal phase type, growth, and purity of the fabricated sample. The primary examinations were performed utilizing profiles coordinating with consistent scale factors. Red lines are the noticed intensities; the dark lines are the determined

information; the blue lines are the distinction: Yobs-Ycalc. The Bragg reflection positions are shown by blue and red bars for cubic and hexagonal periods of  $\text{Yb}_2\text{V}_2\text{O}_7$ , individually. The examples fitted well with the cubic construction. The outcomes showed that the example had a cubic  $\text{Yb}_2\text{V}_2\text{O}_7$  crystal structure with space bunch  $\text{Fd}\bar{3}\text{m}$ . Additionally, it was observed that there was the modest quantity of the hexagonal precious stone construction with  $\text{P3}_1$  space bunch as an impurity.

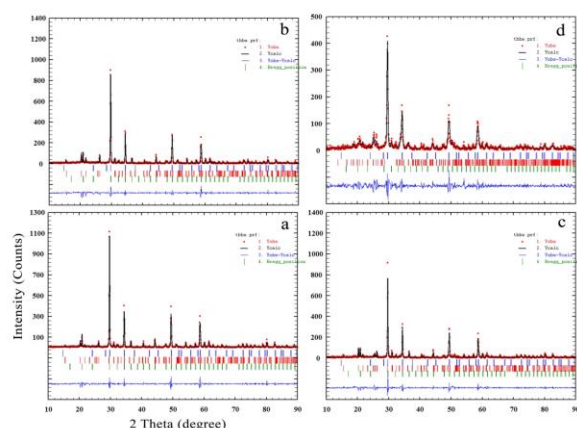


Figure 1.  $\text{Yb}_2\text{V}_2\text{O}_7$  PXR D Patterns and the Rietveld Analyses of (a) S1, (b) S2, (c) S3, and (d) S4.

Table 1 presents the grain size (D) of the acquired nanomaterials in various process temperatures determined employing Scherrer condition (1). In the situation, D is the whole thickness of the translucent example,  $\lambda$  is the X-ray diffraction frequency (0.154 nm), and Scherrer consistent is defined by the k parameter (0.9), the full width at half of its most extreme intensity is characterized by  $B_{1/2}$  of FWHM and the half diffraction point at which the peak is defined by h parameter. The information referenced in Table 1 reveals that by expanding the experiment temperature, the grain size is expanded from S<sub>1</sub> to S<sub>4</sub>.

$$D \text{ (nm)} = K\lambda/B_{\text{hkl}} \cos\theta \quad (1)$$

For this reason, we utilized formula 1, Scherrer condition, picking a peak at around  $29.6^\circ$  and determining the crystallite size. As indicated by Table 1, it was observed that the crystallite sizes were expanded with expanding the experiment temperature.

Table 1. Scherrer data information for  $\text{Yb}_2\text{V}_2\text{O}_7$  compounds.

| Data           | $2\theta$ | $\theta$ | $B_{1/2} (^\circ)$ | $B_{1/2} \text{ (rad)}$ | $\cos\theta_B$ | Crystal size (nm) |
|----------------|-----------|----------|--------------------|-------------------------|----------------|-------------------|
| S <sub>1</sub> | 29.6541   | 14.82705 | 0.29893            | 0.005214                | 0.96670        | 28                |
| S <sub>2</sub> | 29.6417   | 14.82085 | 0.28160            | 0.004912                | 0.96673        | 29                |
| S <sub>3</sub> | 29.6431   | 14.82155 | 0.29907            | 0.005217                | 0.96673        | 27                |
| S <sub>4</sub> | 29.5446   | 14.77230 | 0.28618            | 0.004992                | 0.96695        | 29                |

Table 2 shows the cell boundaries information for  $\text{Yb}_2\text{V}_2\text{O}_7$  got by the Rietveld investigation. The data show that an increase in the experiment temperature makes an expansion in the cell boundaries. Additionally, the table shows the  $R_f$ , Bragg  $R_b$  variables,

and  $\chi^2$  to confirm the decency of the refinements. It was observed that experiment temperature is a fundamental element in the crystal phase growth development and the purity of the acquired compounds. It was observed that the cell boundary amount was expanded when the test temperature was expanded. Moreover, the purity of the cubic crystal phase was improved. When the test temperature was expanded to  $600^\circ\text{C}$  at 8h, the count amount and phase purity were diminished. It shows that the compound is more steady at lower temperatures.

Table 2. Lattice parameter values for the fabricated  $\text{Yb}_2\text{V}_2\text{O}_7$  compounds.

| Sample         | Cell parameters (Å) | $R_f$ | $R_b$ | $\chi^2$ | Count | Cubic phase purity (%) |
|----------------|---------------------|-------|-------|----------|-------|------------------------|
|                | A                   |       |       |          |       |                        |
| S <sub>1</sub> | 10.42714            | 1.82  | 1.92  | 1.92     | 1126  | 89                     |
| S <sub>2</sub> | 10.43151            | 1.74  | 2.61  | 1.98     | 908   | 84                     |
| S <sub>3</sub> | 10.43099            | 1.35  | 2.87  | 2.00     | 924   | 87                     |
| S <sub>4</sub> | 10.46498            | 1.87  | 1.99  | 2.08     | 427   | 81                     |

FESEM pictures of the acquired samples are presented in Figure 2. It is obvious from the pictures that when the test temperature was  $300^\circ\text{C}$ , the material morphology was predominantly porous and the homogeneous nature of the size and morphology of the  $\text{Yb}_2\text{V}_2\text{O}_7$  compound was confirmed. The data indicated that the diameter size of the samples was around 40-50 nm. With expanding the reaction temperature to  $400^\circ\text{C}$ , the morphology of the material was as yet porous. Notwithstanding, the porosity of the got targets was expanded. Whenever the test temperature was expanded to  $500^\circ\text{C}$ , the morphology of the example was molecule and plate. It was observed that the molecule sizes decreased to around 20-30 nm. Additionally, it was observed that when the response temperature was expanded to 600 h, the material morphology was a multigonal particle. The molecule sizes were around 20-40 nm.

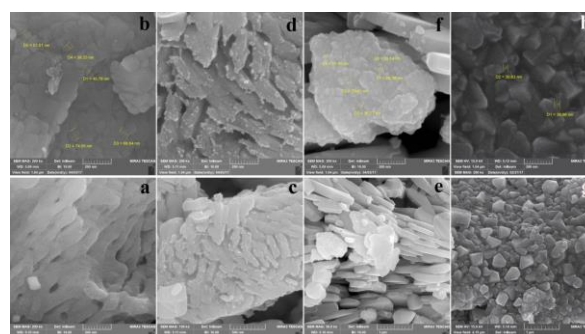


Figure 2. FESEM Pictures of a,b)S1, c,d)S2, e,f)S3 and g,h)S4.

### 2.3. Experimental Design and Accomplishing Ideal Circumstances in MG Corruption Process

There are a lot of trial plans in references to investigate the ideal level of the variables influencing a synthetic experiment. One of the normal plans is the full factorial plan [19, 20] which is characterized by all potential

blends of the elements and their settings. Suppose that there are  $k$  exploring factors and that each parameter is set to  $m$  various levels. The number of potential blends of the elements and their settings will then, at that point, be  $m^k$ . In synthetic frameworks, three levels of the element sets are common and such plans grant the assurance of every principle impact and all cooperation impacts with a modest number of tests.

The connection between variables and reaction is hypothetically displayed by a capacity that is the basic actual component of the issue being scrutinized. This connection makes the reproducibility of the peculiarity under study the option to explore different avenues regarding it and to decipher the outcomes. Response surface methodology (RSM) is a numerical and measurable technique, which investigates exploratory plans by applying an exact model [19]. The sufficiency of the applied model is actually looked at utilizing analysis of variance (ANOVA) [20] which needs some recreate tests. In our work, in toxin paint corruption, the objective was to decide the amount of nanocatalyst that ought to be utilized. Besides, the time and temperature values for the debasement ought to be observed. The response was the acquired debasement ( $Y\%$ ). Various potential blends of these elements were planned which are detailed in Table 3. The examinations were done over two days with arbitrary requests. The noticed information of the factorial plan was fitted to a straight reaction model. Preceding the investigation, low and high element levels were coded to  $-1$  and  $+1$ , separately. Equation 2 shows the connection between the elements and the yield of the response,  $Y\%$ , based on the first request model:

$$Y = +69.18 + 9.91A + 7.24B + 17.23C + 1.37AB - 11.13AC - 3.63BC - 1.68A^2 - 4.86B^2 - 7.98C^2$$

The optimized values of the parameters that affect the photocatalytic reaction yield are shown in Figure 3. Figure 4 presents the normal plot and anticipated corruption yield versus actual information for the  $Yb_2V_2O_7$  test. As could be found from the plots, obviously the information is on a straight line and no self-evident and impressive deviation is found among genuine and anticipated outcomes. To represent the impacts in the above models, the three-layered (3D) reaction surfaces plot of the reaction (utilizing condition (2) when how much time was fixed at the ideal level and the other two parameters, catalyst and  $H_2O_2$ , were permitted to fluctuate) is displayed in Figure 5. To examine the intelligent impacts of three compelling elements on the suggested interaction, the reaction surface procedure (RSM) was utilized. Figure 5 addresses the 3D plots connected with the communication of AC, AB, and BC wherein A is  $H_2O_2$ , B is catalyst amount and C is the response time. The semi-curvature of these plots showed the association between the factors. As such, as mixing time,  $H_2O_2$ , and catalyst amount increment, the colors evacuation rate

improved. This actually intends that the mass exchange of color particles improves on the outer layer of the catalyst and the color adsorption process on the catalyst arrives at harmony state rapidly. Additionally, by expanding the catalyst amount, more surface area of the catalyst is accessible for colors particles catalyst which improves the colors expulsion rate.

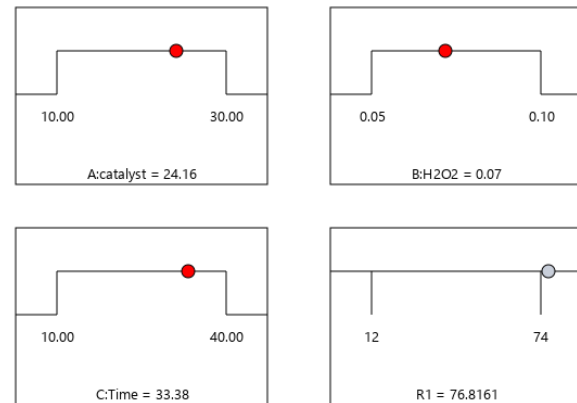


Figure 3. Ramp Data for the MG Degradation Process.

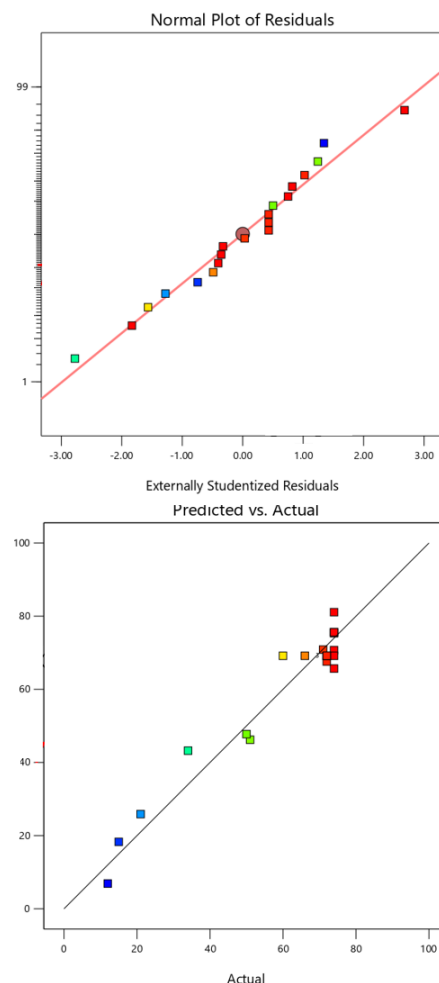


Figure 4. Left) Normal Plot Residuals and Right) Predicted Versus Actual Plots for the Removal of MG dye.

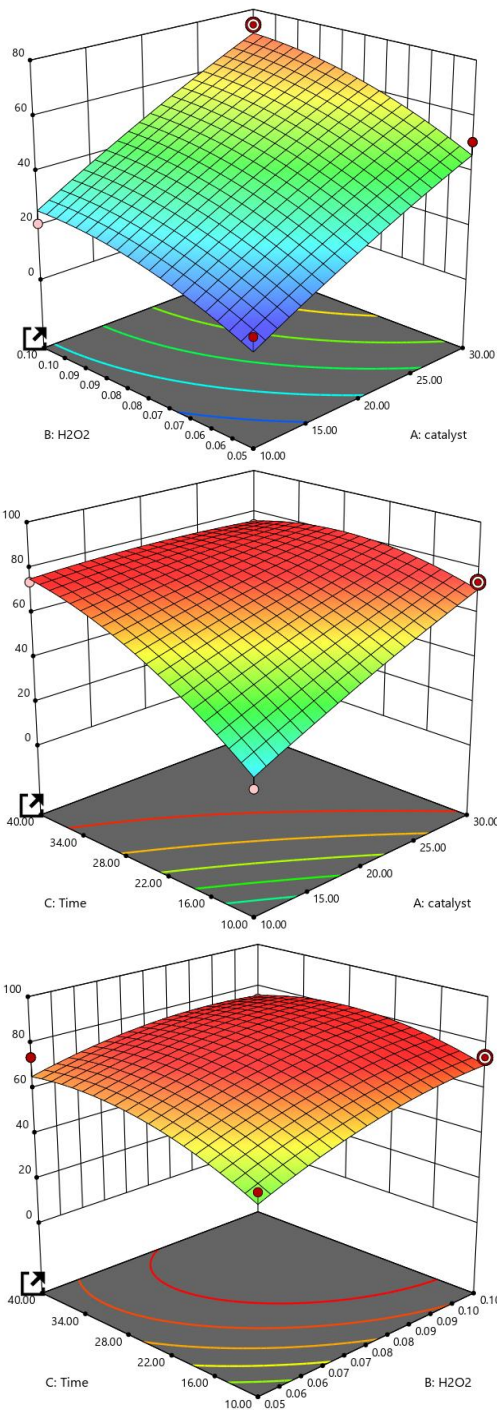


Figure 5. 3D Surface Plots for the Removal of MG dye Under the Photocatalytic Reactions.

In the current work, the advancement of the proposed methodology given the as-incorporated nano impetus (S1) was displayed by the central composite design (CCD) method. The CCD method with three-level and three elements (H<sub>2</sub>O<sub>2</sub> (A), impetus (B), and time (C)) was utilized to examine the impacts of variables. The test reach and levels of free factors are displayed in Table 4. The state of 20 analyses planned by CCD went with to color corruption rate (reaction (Y%)) are present in Table 4. As displayed in Table 4,

the autonomous factors (H<sub>2</sub>O<sub>2</sub> volume (A), impetus sum (B), and blending time (C)) are given the coded structure (- $\alpha$ , -1, 0, +1, + $\alpha$ ).

Table 3. Experimental Results Based on the Proposed Model for Photo-Catalytic MG Degradation by Yb<sub>2</sub>V<sub>2</sub>O<sub>7</sub> Photocatalyst.

| Catalyst | H <sub>2</sub> O <sub>2</sub> | Time | Yield |
|----------|-------------------------------|------|-------|
| 30       | 0.1                           | 10   | 79    |
| 20       | 0.08                          | 25   | 72    |
| 3        | 0.08                          | 25   | 50    |
| 20       | 0.08                          | 25   | 72    |
| 20       | 0.08                          | 25   | 74    |
| 10       | 0.05                          | 40   | 71    |
| 20       | 0.08                          | 25   | 72    |
| 37       | 0.08                          | 25   | 74    |
| 30       | 0.05                          | 10   | 51    |
| 10       | 0.05                          | 10   | 12    |
| 20       | 0.08                          | 50   | 74    |
| 20       | 0.03                          | 25   | 34    |
| 20       | 0.08                          | 25   | 66    |
| 30       | 0.1                           | 40   | 74    |
| 20       | 0.08                          | 0    | 15    |
| 10       | 0.1                           | 40   | 74    |
| 30       | 0.05                          | 40   | 74    |
| 20       | 0.12                          | 25   | 72    |
| 10       | 0.1                           | 10   | 21    |

Table 4. Ranges of Proposed Parameters According to CCD Model.

| Name                                | Lower Limit | Upper Limit | Lower Weight | Upper Weight | Importance |
|-------------------------------------|-------------|-------------|--------------|--------------|------------|
| <b>A:catalyst</b>                   | 10          | 30          | 1            | 1            | 3          |
| <b>B:H<sub>2</sub>O<sub>2</sub></b> | 0.05        | 0.1         | 1            | 1            | 3          |
| <b>C:Time</b>                       | 10          | 40          | 1            | 1            | 3          |

As should have been visible from the ANOVA results recorded in Table 5, the p-worth of the relapse was less than 0.05. This demonstrated that the designed model was huge at a significant degree of certainty (95%). The p-value of the absence of fit was likewise more prominent than 0.05, which affirmed the meaning of the model. Likewise, the coefficient of assurance (the R-square, changed R-square) was utilized to communicate the nature of the quadratic model condition. For this situation, R<sup>2</sup> of variety fitting for Y% 77 showed a serious level of relationship between the reaction and the autonomous variables (R<sup>2</sup> = 0.94). The high worth of the changed relapse coefficient (R<sup>2</sup>-adj = 0.89) was additionally one more file for the high meaning of the suggested model. This intended that the distinction between the trial and the anticipated reactions was negligible. Likewise, the anticipated R-squared worth (0.68) was sensible which shows the high precision and dependability of the created model in the assurance of reaction values.

Table 5. ANOVA Results Based on the Proposed CCD Model for Degradation of MG Using Yb<sub>2</sub>V<sub>2</sub>O<sub>7</sub> Photocatalyst.

| Source            | Sum of Squares | df | Mean Square | F-value | p-value  |             |
|-------------------|----------------|----|-------------|---------|----------|-------------|
| <b>Model</b>      | 8329.80        | 9  | 925.53      | 19.59   | < 0.0001 | significant |
| <b>A-catalyst</b> | 1341.68        | 1  | 1341.68     | 28.40   | 0.0003   |             |

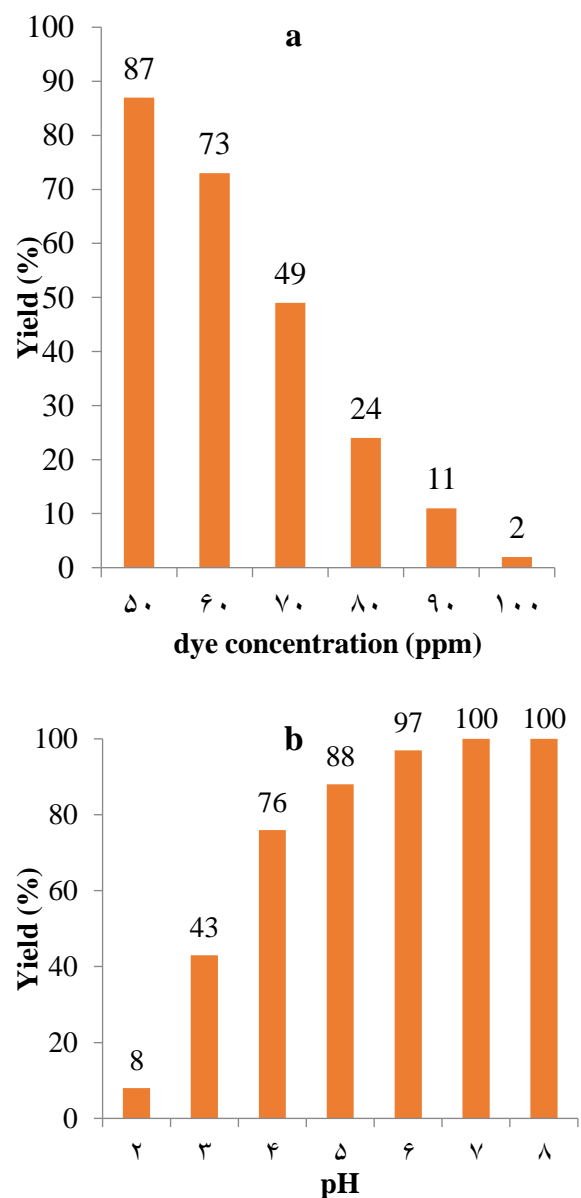
| Source                          | Sum of Squares | df | Mean Square | F-value | p-value  |                 |
|---------------------------------|----------------|----|-------------|---------|----------|-----------------|
| B-H <sub>2</sub> O <sub>2</sub> | 716.33         | 1  | 716.33      | 15.16   | 0.0030   |                 |
| C-Time                          | 4038.54        | 1  | 4038.54     | 85.49   | < 0.0001 |                 |
| AB                              | 15.13          | 1  | 15.13       | 0.3202  | 0.5840   |                 |
| AC                              | 990.13         | 1  | 990.13      | 20.96   | 0.0010   |                 |
| BC                              | 105.13         | 1  | 105.13      | 2.23    | 0.1666   |                 |
| A <sup>2</sup>                  | 40.83          | 1  | 40.83       | 0.8642  | 0.3745   |                 |
| B <sup>2</sup>                  | 341.19         | 1  | 341.19      | 7.22    | 0.0228   |                 |
| C <sup>2</sup>                  | 904.15         | 1  | 904.15      | 19.14   | 0.0014   |                 |
| Residual                        | 472.40         | 10 | 47.24       |         |          |                 |
| Lack of Fit                     | 331.07         | 5  | 66.21       | 2.34    | 0.1859   | not significant |
| Pure Error                      | 141.33         | 5  | 28.27       |         |          |                 |
| Cor Total                       | 8802.20        | 19 |             |         |          |                 |

The preparation of the 50 ppm MG color arrangement was done by mixing 50 MG powder in 1000 mL of pure water. The pH of the acquired arrangement was 4. As indicated by Table 3, in a normal test, a certain amount (g) of the as-fabricated Yb<sub>2</sub>V<sub>2</sub>O<sub>7</sub> (S<sub>1</sub>) photocatalyst was poured into 70 mL of MG stock solution and sonicated for 10 min in a dark space to lay out an adsorption/desorption balance between MG molecules and the outer layer of the photocatalyst. A short time later, a certain volume (mL) of H<sub>2</sub>O<sub>2</sub> was added to the solution mixture, trailed by attractive blending under normal light. Whenever the planned time (min) was slipped by, the solution was filtered and the photocatalyst was isolated by centrifugation to gauge the retention spectra of MG and ascertain the MG focus utilizing UV-Vis spectrophotometry. The photodegradation (%) of MG was determined by the accompanying recipe:

$$\left(\frac{A_0 - A_t}{A_0}\right) \times 100 \quad (3)$$

in which, the absorbance of MG at time 0 and t, was defined by A<sub>0</sub> and A<sub>t</sub>, respectively. Figure 6 shows the color debasement graphs for the got materials in the ideal circumstances. Figure 6a shows the impact of color fixation on the corruption yield. Obviously, by expanding the color fixation to 60 ppm, the corruption of color was increased. Notwithstanding, the corruption was diminished the dye concentration was expanded up to 70 ppm. It appears that the light frequency can not be entered into the dye solution when the dye concentration is high and so the photocatalytic action can not be begun productively. Figure 6b shows the color volume impact on the corruption yield. It was observed that at 50 mL dye volume, the corruption was almost finished; when the volume was 50 and 60 mL, the debasement was high. Maybe, by expanding the dye volume up to 70 mL, the yield was diminished extensively. It tends to be because of the diminishing adsorption of dye on the material causing the interaction to be gone on leisurely. Figure 6c shows the impact of pH value on the corruption yield. MG solution pH was 4. It was observed that at acidic pH

values (2-4), the corruption yield was little. Notwithstanding, when the pH was expanded up to 10, by adding 0.01M NaOH arrangement, the corruption yield was expanded and the debasement value was 100% at pH=5.5 to 10. It may be because of the existence and expanded measure of OH<sup>-</sup> in the solution causing the interaction to be gone quickly. The reusability performance of S<sub>1</sub> is presented in Figure 6d. It demonstrates that the fabricated catalyst shows high reusability execution for the interaction until run 3. In any case, the synergist performance was diminished impressively when the recovery of the catalyst was accomplished more. It is expected to the failure of the catalyst to adsorb the color on a superficial level. Figure 6 d presents the photodegradation of MG by synthesized and raw materials. It shows that the degradation yield for Yb<sub>2</sub>V<sub>2</sub>O<sub>7</sub> is high.



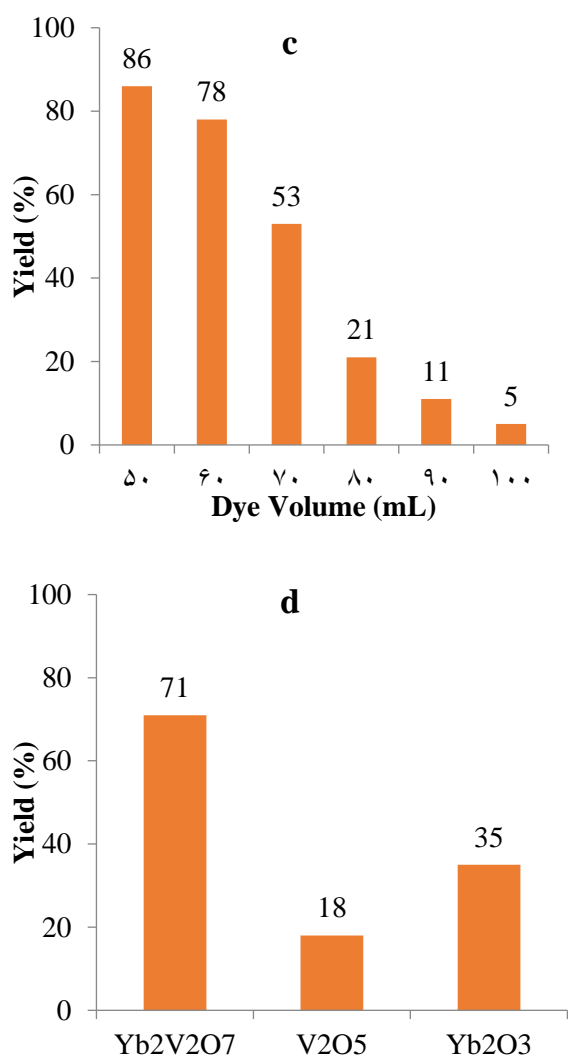


Figure 6. MG Degradation (%) at (a) Different dye Concentrations, (b) Different Solution pH, (c) Different dye Volumes, and (d) Experiments for the MG Degradation Versus Synthesized and Raw Materials.

## Conclusion

In the current work, the photocatalytic execution of Yb<sub>2</sub>V<sub>2</sub>O<sub>7</sub> to eliminate toxin dye was prepared. The photocatalytic information showed that the got materials had astounding proficiency for the expulsion of MG from the watery arrangement. The ideal circumstances were gotten by the experimental design program. It was observed that the ideal condition was 0.07 mL H<sub>2</sub>O<sub>2</sub>, 0.02 g catalyst, 40 min. The yield in the condition was 77 %.

## Acknowledgment

The authors extend their appreciation to the Deanship of Scientific Research at King Khalid University for funding this work through a group research program under grant number RGP. 2/129/42

## Reference

- [1] Srivastava S., Sinha R., Roy D., (2004), Toxicological effects of malachite green. *Aquatic toxicol.* 66: 319-329.  
<https://doi.org/10.1016/j.aquatox.2003.09.008>
- [2] Tolia J., Chakraborty M., Murthy Z., (2012), Photocatalytic degradation of malachite green dye using doped and undoped ZnS nanoparticles. *Pol. J. Chem. Technol.* 14: 16-21.  
DOI: <https://doi.org/10.2478/v10026-012-0065-6>
- [3] Chen C., Lu C., Chung Y., Jan J., (2007), UV light induced photodegradation of malachite green on TiO<sub>2</sub> nanoparticles. *J. Hazard. Mater.* 141: 520-528.  
<https://doi.org/10.1016/j.jhazmat.2006.07.011>
- [4] Sharma J., Sharma S., Vineet Soni V., (2023). Toxicity of malachite green on plants and its phytoremediation: A review. *Regional Studies in Marine Science.* 62, 102911.  
<https://doi.org/10.1016/j.rsma.2023.102911>
- [5] Miranzadeh M., Afshari F., Khataei B., Kassae M., (2020), Adsorption and photocatalytic removal of arsenic from water by a porous and magnetic nanocomposite: Ag/TiO<sub>2</sub>/Fe<sub>3</sub>O<sub>4</sub>@GO. *Adv. J. Chem.* A. 3: 408-421.  
<https://doi.org/10.33945/SAMI/AJCA.2020.4.3>
- [6] Sajjadnejad M., Karimi Abadeh H., (2020), Processing of nanostructured TiO<sub>2</sub> and modification of its photocatalytic behavior for methylene blue degradation. *Adv. J. Chem. A.* 3: 422-431.  
<https://doi.org/10.33945/SAMI/AJCA.2020.4.4>
- [7] Hu K.-h., Meng M., (2013), Degradation of malachite green on MoS<sub>2</sub>/TiO<sub>2</sub> nanocomposite. *Asian J. Chem.* 25: 5827-5829.  
<https://doi.org/10.14233/ajchem.2013.OH102>
- [8] Hamad, H., & Moustafa, M. T. (2023). Optimization study of the adsorption of malachite green removal by MgO nano-composite, nano-bentonite and fungal immobilization on active carbon using response surface methodology and kinetic study. *Environmental Sciences Europe*, 35(1), 1-37.  
<https://doi.org/10.1186/s12302-023-00728-1>
- [9] Bansal P., Bhullar N., Sud D., (2009), Studies on photodegradation of malachite green using TiO<sub>2</sub>/ZnO photocatalyst. *Desalin. Water Treat.* 12: 108-113.  
<https://doi.org/10.5004/dwt.2009.944>
- [10] Soni H., Ji N. K., (2014), UV light induced photocatalytic degradation of malachite GREEN on TiO<sub>2</sub> nanoparticles. *Int. J. Recent Res. Rev.* 7: 10-15.  
<https://doi.org/10.1016/j.jhazmat.2006.07.011>
- [11] Sols-Casados D., Escobar-Alarcón L., Fernández M., Valencia F., (2013), Malachite green degradation in simulated wastewater using Ni<sub>x</sub>: TiO<sub>2</sub> thin films. *Fuel.* 110: 17-22.  
<https://doi.org/10.1016/j.fuel.2012.10.042>
- [12] Khezami L., Taha K. K., Ghiloufi I., El Mir L., (2016), Adsorption and photocatalytic degradation of malachite green by vanadium doped zinc oxide nanoparticles. *Water Sci. Technol.* 73: 881-889.  
<https://doi.org/10.2166/wst.2015.555>
- [13] Jo W.-K., Parka G. T., Tayade R. J., (2014), Synergetic effect of adsorption on degradation of malachite green dye under blue LED illumination using spiral-shaped

- photocatalytic reactor. *J. Chem. Technol. Biotechnol.* 90: 2280-2289.  
<https://doi.org/10.1002/jctb.4547>
- [14] He H-Y., (2015), Photocatalytic degradations of malachite green on magnetically separable Ni<sub>1-x</sub>Co<sub>x</sub>Fe<sub>2</sub>O<sub>4</sub> nanoparticles synthesized by using a hydrothermal process. *Amer. Chem. Sci. J.* 6: 58-68.  
DOI: <https://doi.org/10.9734/ACSj/2015/14764>
- [15] Afshar S., Samari Jahromi H., Jafari N., Ahmadi Z., Hakamizadeh M., (2011), Degradation of malachite green oxalate by UV and visible lights illumination using Pt/TiO<sub>2</sub>/SiO<sub>2</sub> nanophotocatalyst. *Sci. Iran.* 18: 772-779.  
<https://doi.org/10.1016/j.scient.2011.06.007>
- [16] Khademinia S., Behzad M., Kafi-Ahmadi L., Hadilou S., (2018), Hydrothermally synthesized strontium arsenate nanomaterial through response surface methodology. *Z. Anorg. Allg. Chem.* 644: 221-227.  
<https://doi.org/10.1002/zaac.201800004>
- [17] Hosseiny Davarani S. S., Rezayati zad Z., Taheri A. R., Rahmatian N., (2017), Highly selective solid phase extraction and preconcentration of Azathioprine with nano-sized imprinted polymer based on multivariate optimization and its trace determination in biological and pharmaceutical samples. *Mater. Sci. Eng. C.* 71: 572-583.  
<https://doi.org/10.1016/j.msec.2016.09.075>
- [18] Abdollahi F., Taheri A., Shahmari M., (2019), Application of selective solid-phase extraction using a new core-shell-shell magnetic ionimprinted polymer for the analysis of ultra-trace mercury in serum of gallstone patients. *Sep. Sci. Technol.*  
<https://doi.org/10.1080/01496395.2019.1651337>
- [19] Hosseiny Davarani S. S., Rezayati zad Z., Taheri A. R., Rahmatian N., (2017), Highly selective solid phase extraction and preconcentration of Azathioprine with nano-sized imprinted polymer based on multivariate optimization and its trace determination in biological and pharmaceutical samples. *Mater. Sci. Eng. C.* 71: 572-583.  
<https://doi.org/10.1016/j.msec.2016.09.075>
- [20] Abdollahi F., Taheri A., Shahmari M., (2019), Application of selective solid-phase extraction using a new core-shell-shell magnetic ionimprinted polymer for the analysis of ultra-trace mercury in serum of gallstone patients. *Sep. Sci. Technol.*  
<https://doi.org/10.1080/01496395.2019.1651337>